

ON THE EXISTENCE OF BROWN DWARFS MORE MASSIVE THAN THE HYDROGEN BURNING LIMIT

JOHN C. FORBES AND ABRAHAM LOEB

Astronomy Department, Harvard University, 60 Garden St., Cambridge MA 02138, USA;
john.forbes@cfa.harvard.edu, aloeb@cfa.harvard.edu

Draft version June 12, 2022

ABSTRACT

Almost by definition brown dwarfs are objects with masses below the hydrogen burning limit, around $0.07M_{\odot}$. Below this mass, objects never reach a steady state where they can fuse hydrogen. Here we demonstrate, in contrast to this traditional view, that brown dwarfs with masses greater than the hydrogen burning limit may in principle exist in the universe. These objects, which we term “overmassive brown dwarfs” form a continuous sequence with traditional brown dwarfs in any property (mass, effective temperature, radius, luminosity). To form an overmassive brown dwarf, mass must be added sufficiently slowly to a sufficiently old traditional brown dwarf below the hydrogen burning limit. We identify mass transfer in binary brown dwarf systems via Roche lobe overflow driven by gravitational waves to be the most plausible mechanism to produce the bulk of the putative overmassive brown dwarf population.

Keywords: binaries: general, brown dwarfs, stars: evolution, stars: low-mass

1. INTRODUCTION

The process which forms stars out of molecular clouds produces objects over a wide range of masses, with an abundance peak around $0.2 M_{\odot}$ (e.g. Chabrier 2003). In the course of their formation, stars contract gravitationally, heating up their interiors until the conditions are right for the fusion of hydrogen. At this point (modulo interim phases involving deuterium fusion), the contraction is halted and the star settles into a steady state structure, which changes very gradually as the star converts hydrogen to heavier elements. Below a critical mass, which we shall denote M_{HBL} for the “hydrogen burning limit,” this process of collapse never yields conditions for which the power generated by nuclear fusion can supply the star’s surface luminosity. The core of the star becomes supported by electron degeneracy pressure, and the sub-stellar object (a brown dwarf) cools and contracts on a thermal timescale (Kumar 1963; Hayashi & Nakano 1963).

Since the first studies in the 1960s, research on brown dwarfs was re-energized in the 1990s by their observational discovery (Rebolo et al. 1995). Continuous comparison with data has led to improving evolutionary models (Laughlin & Bodenheimer 1993; Burrows et al. 1993; Saumon et al. 1994; Baraffe et al. 1995; Tsuji et al. 1996; Burrows et al. 1997; Allard et al. 1997; Chabrier & Baraffe 1997; Chabrier et al. 2000; Burrows et al. 2001; Baraffe et al. 2003; Saumon & Marley 2008; MacDonald & Mullan 2009; Baraffe et al. 2015) with much of the modeling uncertainty associated with the atmospheres and the influence of clouds (e.g. Ackerman & Marley 2001; Cushing et al. 2008; Morley et al. 2012; Marley & Robinson 2015).

The distinction between brown dwarfs and low-mass stars is often taken to be set by mass. There are a number of difficulties with this definition, however. First, masses are difficult to derive observationally. Second, the hydrogen burning limit has a well-known dependency on metallicity (e.g. Chabrier & Baraffe 1997), with higher metal-

licity corresponding to a lower M_{HBL} . Third, as we will show in this work, objects that behave like brown dwarfs may in principle exist with masses exceeding M_{HBL} . We therefore recommend that brown dwarfs be defined more by their composition: hydrogen-rich substellar objects that do not fuse hydrogen.

In this work we will proceed as follows. First, we present a modest extension of the classical analytic model used to estimate M_{HBL} in section 2. Then in section 3 we show that this analytic model has an interesting heretofore unrecognized consequence, namely that brown dwarfs may exist with masses exceeding M_{HBL} . In this section we make predictions for the properties of these objects. We discuss the implications and prospects for observational tests in section 4 then summarize our conclusions in section 5.

2. THE HYDROGEN BURNING LIMIT

Recently Auddy et al. (2016) updated the classical analytic model for the hydrogen burning limit from Burrows & Liebert (1993). In this section we will apply this model to predict the critical mass dividing hydrogen burning stars from brown dwarfs as a function of metallicity. The basic premise of these models is that the nuclear luminosity L_N must match the surface luminosity L_S . In the course of their collapse, many objects will burn deuterium and even hydrogen for some time, but to be considered a main sequence star, the object must eventually reach an equilibrium with $L_S = L_N$. The other key ingredient of the model connecting the surface and the core is that energy in objects within the relevant mass range is nearly entirely transported by convection as opposed to radiation (or conduction). This means that the star can be modeled as a constant-entropy polytrope with index $n = 1.5$, plus some additional accounting for the change in entropy resulting from the transition between the partially ionized core and the molecular photosphere.

2.1. Surface Luminosity

The surface luminosity can be written $L_S = 4\pi R^2 \sigma T_{\text{eff}}^4$, where σ is the Stefan-Boltzmann constant, R is the stellar radius, and T_{eff} is the effective temperature. Using a polytropic equation of state where the normalization is set accounting for the degeneracy pressure, Auddy et al. (2016) arrive at the relation

$$R = 2.80858 \times 10^9 \text{ cm} (M/M_\odot)^{-1/3} \mu_e^{-5/3} (1 + \gamma + \alpha\psi), \quad (1)$$

where M is the total mass of the star, $1/\mu_e = X + Y/2$ is the number of nucleons per electron, with X and Y defined as the mass fractions of hydrogen and helium respectively, and $(1 + \gamma + \alpha\psi)$ is a correction factor accounting for degeneracy. In particular ψ is the ratio of the characteristic thermal energy per particle $k_B T$, the Boltzmann constant times the temperature, to the electron Fermi energy μ_F . This is multiplied by the ratio $\alpha = 5\mu_e/2\mu_1$, where $1/\mu_1 = ((1 + x_{H^+})X + Y/4)$ is the mean molecular weight for a gas with an ionization fraction x_{H^+} . Finally, γ is a function of ψ

$$\gamma = -\frac{5}{16} \psi \ln(1 + e^{-1/\psi}) + \frac{15}{8} \psi^2 \left(\frac{\pi^2}{3} + \text{Li}_2(-e^{-1/\psi}) \right), \quad (2)$$

where Li_2 is the polylogarithm function of order 2.

The effective temperature is derived by assuming that the photosphere lies at an optical depth of $\tau = 2/3$ with a constant Rosseland mean opacity, κ_R . Combining this approximation with a prescribed entropy jump between the core and the surface from Chabrier et al. (1992) yields an effective pressure from which one can back out an effective density and temperature (see Auddy et al. (2016) for more details), namely,

$$\left(\frac{\rho}{1 \text{ g cm}^{-3}} \right)^{1.4} = \frac{6.89811}{\kappa_R N_A k_B} \left(\frac{M}{M_\odot} \right)^{5/3} \frac{\mu_e^{10/3} \mu_2}{(1 + \gamma + \alpha\psi)^2 \psi^{1.58}}, \quad (3)$$

where dimensional quantities on the right hand side are all evaluated in CGS units, $1/\mu_2 = X/2 + Y/4$, and

$$T_{\text{eff}} = 2.57881 \times 10^4 \text{ K} \kappa_R^{-2/7} \left(\frac{M}{M_\odot} \right)^{10/21} \frac{\mu_e^{20/21} \mu_2^{2/7} \psi^{8/7}}{(1 + \gamma + \alpha\psi)^{4/7}}, \quad (4)$$

again with κ_R in CGS units. These equations yield an expression¹ for L_S as a function of κ_R , ψ , M , X , and Y ,

$$L_S = 0.6118 L_\odot \kappa_R^{-8/7} (M/M_\odot)^{26/21} \frac{\psi^{32/7} \mu_e^{10/21} \mu_2^{8/7}}{(1 + \gamma + \alpha\psi)^{2/7}}. \quad (5)$$

Given a particular value of Z , we assume that $Y = Y_p + fZ$, where $Y_p = 0.24$ and $f = 2$, leaving $X = 1 - Y - Z$. For now we leave M and ψ as free parameters. The opacity, however, is itself a function of density, temperature, and composition, i.e.

$$\kappa_R = \kappa_R(\rho, T, X, Z). \quad (6)$$

In the analytic models, κ_R is left fixed, but here we attempt to make the model more self-consistent by iteratively searching for a value of κ_R such that equations

(3), (4), and (6) are simultaneously satisfied at the surface of the star. If the functional form of the opacity is a power-law in ρ and T , these equations may be solved analytically. We iterate numerically instead in order to accommodate more general opacity laws. For consistency with the MESA models, we use the tables from Ferguson et al. (2005), but of course other opacity laws may be substituted in easily.

2.2. Nuclear Luminosity

The surface luminosity must be balanced by the nuclear luminosity L_N in a steady state. According to Burrows & Liebert (1993) and Auddy et al. (2016), low-mass stars do not reach sufficient temperatures to burn all the way through the PPI chain of nuclear reactions, in particular because the ${}^3\text{He}$ nuclei face a much higher Coulomb barrier. The first two reactions in PPI are $p + p \rightarrow d + e^+ + \bar{\nu}_e$ and $p + d \rightarrow {}^3\text{He} + \gamma$. The first reaction limits the rate, while the second takes place quickly and produces roughly 5 times the energy per reaction.

The energy generation rate of each reaction per unit volume is an exponential function of temperature, namely (Fowler et al. 1975)

$$\dot{\epsilon}_{pp} = 2.5 \times 10^6 (\rho X^2 / T_6^{2/3}) e^{-33.8/T_6^{1/3}} \text{ erg g}^{-1} \text{ s}^{-1}, \quad (7)$$

$$\dot{\epsilon}_{pd} = 1.4 \times 10^{24} (\rho X D / T_6^{2/3}) e^{-37.2/T_6^{1/3}} \text{ erg g}^{-1} \text{ s}^{-1}, \quad (8)$$

where the temperature normalization is $T_6 = T/(10^6 \text{ K})$, and the deuterium fraction by mass is D . The fully-convective piecewise-constant-entropy nature of low-mass stars implies that the total nuclear reaction luminosity is (Burrows & Liebert 1993),

$$L_N = \frac{2.4 \dot{\epsilon}_c}{(3u/2 + s)^{3/2}} (M/M_\odot) L_\odot \quad (9)$$

where $\dot{\epsilon}_c$ is the energy generation rate per unit volume at the center of the star in CGS units. In deriving this equation, the energy generation rate in the innermost part of the star has been integrated under the assumption that it may be approximated as a power law, $\dot{\epsilon} \propto T^s \rho^u$. Burrows & Liebert (1993) estimate that in this regime $u = 2 + 1.29 \times H(0)/3$ and $s = 33.8/(3T_6^{1/3}) - 2/3 - 1.29 \times H(0)$, where $H(0) \approx \min(0.977\Gamma^{1.29}, 1.06\Gamma)$ is the log of the screening factor from Graboske et al. (1973), and $\Gamma = 0.227(\rho/\mu_e)^{1/3}/T_6$ (so long as we have specialized to protons and deuterons for which the charge is 1).

To estimate L_N we now need to know the value of $\dot{\epsilon}_c$. For this we simply take $\dot{\epsilon}_{pp} + \dot{\epsilon}_{pd}$, but to evaluate these we need the central temperature and density, and the hydrogen and deuterium abundances. For the former, we use the relevant equations from Auddy et al. (2016),

$$T_c = 7.68097 \times 10^8 (M/M_\odot)^{4/3} \psi \mu_e^{8/3} (1 + \gamma + \alpha\psi)^{-2} \text{ K}, \quad (10)$$

$$\rho_c = 1.28412 \times 10^5 (M/M_\odot)^2 \mu_e^5 (1 + \gamma + \alpha\psi)^3 \text{ g cm}^{-3}. \quad (11)$$

The deuterium fraction is less obvious. In the long-run steady state, the pp and pd reactions are responsible for the continuous creation and destruction of deuterium. It should be noted of course that the initial deuterium abundance is not zero, but may be closer to the primordial value. This issue will be discussed further in the

¹ Auddy et al. (2016) evaluate μ_e at a particular value and absorb the result into the leading constant, but we retain it since it changes along with metallicity.

following section. The equilibrium value of deuterium abundance is taken to be

$$D_{\text{eq}} = 1.79 \times 10^{-18} X e^{3.4/T_6^{1/3}} \frac{Q_{pd}}{Q_{pp}} \quad (12)$$

This equation sets the rate of deuterium formation equal to the rate of destruction, where the reaction rates are taken to be equal to the energy generation rates divided by the energy produced per reaction, with $Q_{pd} = 5.494$ MeV and $Q_{pp} = 1.18$ MeV. Throughout this paper, results are shown assuming solar metallicity.

2.3. The Main Sequence

Having now written down L_N and L_S of stars as a function of M and ψ , we can find the locus of points in the $\psi - M$ plane such that $L_N = L_S$. As originally detailed by Burrows & Liebert (1993), this locus has a minimum M as a function of ψ . Although the value of ψ is deemed moderately unrealistic by Burrows & Liebert (1993) and Auddy et al. (2016), the minimum M identified by this approach corresponds reasonably well with the location of the hydrogen burning limit as identified by more detailed numerical modeling.

Figure 1 illustrates how the analytic model is constructed. Above the $L_N = L_S$ line, given the very high power with which L_N depends on M , the nuclear luminosity exceeds the surface luminosity. Below the $L_N = L_S$ line at any particular ψ , $L_N < L_S$. The mass at which the $L_N = L_S$ curve has a minimum is the canonical dividing line between brown dwarfs and stars. Below this line, objects may burn deuterium and even hydrogen briefly, but they never reach a steady state in which the nuclear luminosity is enough to power the energy being lost at the surface. Above the hydrogen burning limit, stars reach this steady state and may burn hydrogen in their cores for more than 10^{12} years.

In the absence of substantial accretion or winds, stars are restricted to horizontal trajectories in this diagram. Objects generally begin on the right-hand side of this diagram, i.e. $\psi \gtrsim 1$. Before collapsing to form a stellar object, the gas pressure is thermal, and only once the collapse of the object is halted (or at least slowed to a thermal timescale) does the gas begin to be supported by degeneracy pressure. As the object cools, it moves leftwards in the diagram as indicated by the red arrows in Figure 1. Objects above the hydrogen burning limit eventually reach the $L_N = L_S$ line, while below the limit, objects continue to cool.

The point at which stars reach the $L_N = L_S$ line represents an equilibrium point, but we should consider its stability. Objects that fall into the $L_N > L_S$ region must readjust, but if they do so by decreasing ψ , the equilibrium point would not be stable, but rather a saddle point. When $L_N > L_S$ the center of the star is unable to remove the excess of energy generated by the unbalanced L_N , so the center of the star must heat up, increasing ψ and pushing the star rightward as indicated by the blue arrows in Figure 1. Thus the high- ψ branch of the $L_N = L_S$ curve represents a stable equilibrium, and by the same token the low- ψ branch of this curve must be unstable.

2.4. Simulations

To verify the analytic picture presented in the previous section, we have employed MESA, the Modules for Experiments in Stellar Astrophysics (Paxton et al. 2011, 2013, 2015), a modern, flexible, open, and modular stellar evolution code. In this work we use MESA essentially as-is², i.e. we make no changes to the code itself. We also use the default values of all parameters with the following exceptions.

The initial composition of the star is set via `set_uniform_initial_composition=.true.`, with prescribed values of hydrogen, deuterium, and ^3He and ^4He . Metallicities and ^4He abundances are related as discussed in the previous section. The ^2H abundance is set to half the primordial value (Cooke et al. 2016), and the ^3He abundance is set to a fixed fraction, 2.8×10^{-5} , of the ^4He abundance. The parameters `initial_mass`, `initial_y`, and `initial_z` are set to consistent values with the more detailed abundances. For running low-mass stars, we use `which_atm_option='tau_100_tables'` as recommended in Choi et al. (2016), and we use a nuclear reaction net that includes Deuterium burning via `default_net_name='pp_extras.net'`. Finally, the `max_age` and `max_model_number` are set to large enough values that they never cause the runs to terminate.

Essentially, we allow the model to evolve longer than the default since we are interested in the lifetimes of extremely long-lived stars; we use a nuclear reaction network that includes deuterium burning, since this is important at least in the early lives of these stars; and we use an outer boundary condition that avoids some of the difficulty in realistically modeling the atmospheres of very low-mass stars.

We begin by running a set of models closely-spaced in initial stellar mass until each model terminates, generally because it becomes too degenerate for MESA’s equation of state. We run models for masses ranging from $0.05M_\odot$ to $0.09M_\odot$, encompassing the range of predicted values for the mass of the hydrogen burning limit. For comparison to the schematic diagram shown in Figure 1, we extract isochrones in $\psi - M$ space by interpolating output values of ψ and M as a function of age (each model provides data at different age intervals depending on adaptive timestepping).

Figure 2 shows the evolution of these isochrones in intervals equally spaced in $\log(\text{age})$. Models are not included in a given isochrone if they have already terminated at that age. As expected, models begin with large values of ψ . Brown dwarfs, below about $0.071M_\odot$, cool steadily with a very regular leftward march in this diagram. Stars above this mass cool until they reach something resembling the analytic curve, where they pile up and slowly burn hydrogen. Eventually, as these stars deplete the hydrogen in their core (and elsewhere, since they are fully convective), they move back to the right as a result of the changing chemical composition. In particular $\psi \propto \mu_e^{2/3}$ and μ_e increases over time as hydrogen is consumed. For clarity, we only show isochrones up to $10^{12.2}$ years, but the models continue evolving through their post-main-sequence up to a maximum age of 7×10^{12} years just above the hydrogen burning limit. This represents the “end of the main sequence” (Laugh-

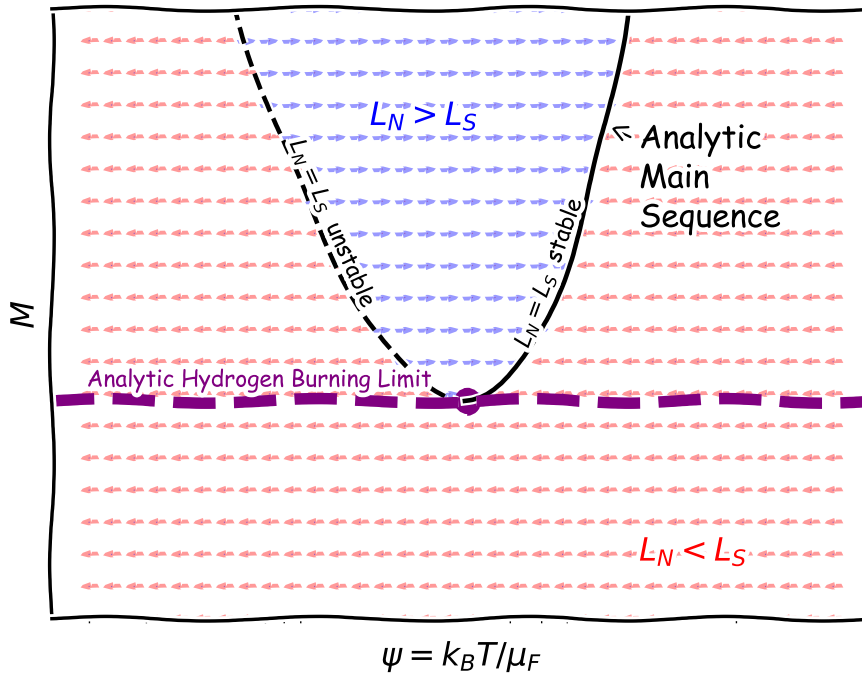


Figure 1. A schematic diagram. The evolutionary arrows represent the evolution of stars or sub-stellar objects that happen to find themselves at a given point in this space, depending on the relative values of the nuclear luminosity L_N and the surface luminosity L_S . The arrows are horizontal, since typically these objects should remain approximately the same mass throughout their lives. The curve where $L_N = L_S$ is shown in black. The minimum value of M for this curve is the hydrogen burning limit, M_{HBL} according to the analytic model used to derive this curve. For $M > M_{\text{HBL}}$, objects start from the right-hand side of the diagram and settle along the solid part of the $L_N = L_S$ curve, which is stable because perturbations off of the curve result in the object’s return to the curve. The left-hand branch of the $L_N = L_S$ curve is unstable, but its existence implies that any object that finds itself to the left of that branch will cool, contract, and never reach the main sequence. It follows that objects that behave like brown dwarfs may in principle exist with masses exceeding M_{HBL} .

lin et al. 1997), i.e. the maximum age of stars³, and the maximum age of these models agrees well with those calculations.

In addition to the isochrones shown in green, we include versions of the analytic model with several different opacity laws which are applied near the surface of the star. The black line assumes an opacity independent of density and temperature, namely $0.02(1 + X) \text{ cm}^2 \text{ g}^{-1}$, one tenth of the opacity appropriate for free electrons. This is a reasonable order of magnitude for the opacity, but the lack of dependence on temperature and density is not realistic. The blue line uses the same opacity law as MESA in this region of T - ρ space, namely the tabulated results of Ferguson et al. (2005). The red line, which comes closest to agreeing with the results of the MESA models, is an opacity similar to but not quite that of H-, which does indeed dominate the opacity at a slightly deeper layer in the star than the photosphere according to the simulations. In particular for this opacity we set $\kappa = 10^{-14} T^4 \text{ cm}^2 \text{ g}^{-1}$. These various versions of the analytic model do not quite agree with the MESA simulations in terms of the exact location of the hydrogen burning limit in M - ψ space, but the qualitative agreement between the schematic diagram in Figure 1 and the behavior of the MESA models is good.

³ This is a quantitative estimate of the newly updated final line of Harvard’s alma mater “Till the stars in the firmament die.”

3. OVERMASSIVE BROWN DWARFS

Thus far we have reviewed the analytic derivation of the location of the hydrogen burning limit, the dividing line between brown dwarfs and stars. For both brown dwarfs and M dwarfs, the existence of the unstable low- ψ branch of the $L_N = L_S$ curve shown in Figure 1 has been completely irrelevant. Brown dwarfs simply cool steadily, and M dwarfs reside on the high- ψ branch before exhausting their supply of hydrogen and moving off to higher ψ . In other words, the typical evolutionary paths of low-mass stars and brown dwarfs never pass near the low- ψ branch.

Despite what happens to the typical star, it is clear from Figure 1 that the analytic model makes the following prediction: *objects with some mass M above the hydrogen burning limit behave like brown dwarfs if their value of ψ is less than the lowest value of ψ for which $L_N = L_S$ at mass M .* In other words, it is possible to have brown dwarfs with masses above the canonical hydrogen burning limit. In what follows we shall explore the properties of these “overmassive brown dwarfs,” evolutionary pathways by which they may arise, and potential observational signatures.

3.1. Properties

In order to understand the properties of such objects, we ran a series of models with MESA to first verify this prediction of the analytic model, and then to study the

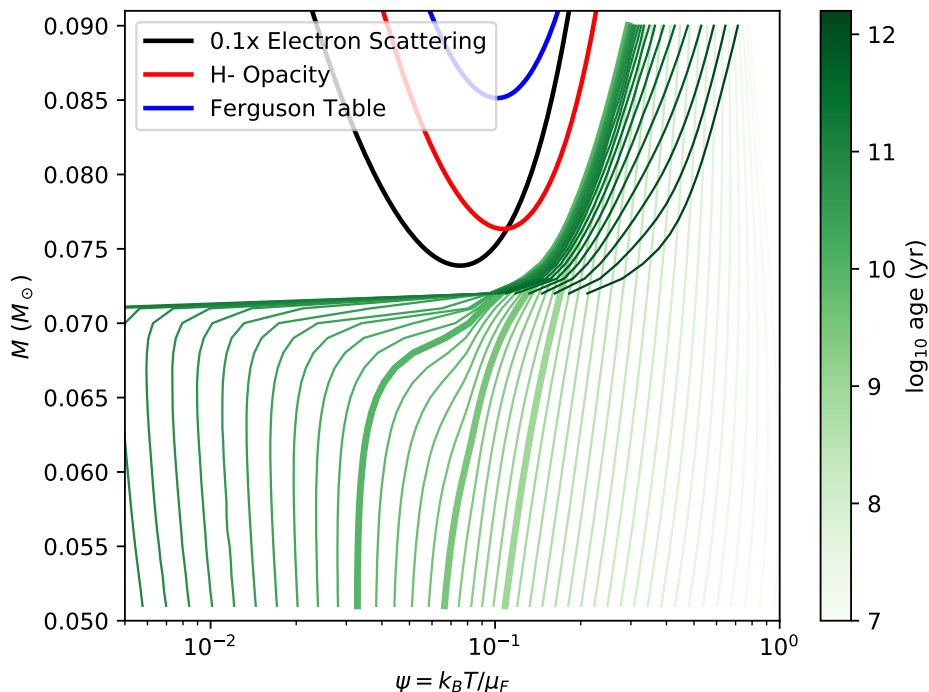


Figure 2. Isochrones and model validation. Three different versions of the analytic model are shown in black, red, and blue – everything is the same between them except the opacity law, as indicated. Plotted for comparison are isochrones spaced in 0.1 dex intervals of age extracted from a library of MESA models, with darker greens corresponding to older ages. Isochrones at 1, 3.1, and 10 Gyr are highlighted. The hydrogen burning limit according to the MESA models appears in this diagram as the mass dividing objects that continuously cool from those that settle on a curve resembling a half-parabola, just as expected from the schematic diagram of Figure 1. While the locations of the main sequence and M_{HBL} do not agree perfectly with the analytic model, there is a remarkable qualitative agreement.

properties of these objects provided they could be reproduced.

Based on the isochrones produced by running MESA straightforwardly for a few dozen closely-spaced initial masses, we found that, as far as MESA is concerned in this configuration for this set of parameters, the hydrogen burning limit is about $M_{\text{HBL}} = 0.071M_{\odot}$. We therefore copied the highest-mass MESA model from this mass library, namely the one with $M = 0.07M_{\odot}$, and terminated it prematurely by setting the MESA parameter `eta_center_limit` to 10 different values starting at 1 and increasing in increments of 0.2 dex. This parameter will terminate the MESA run when $\eta = 1/\psi$ exceeds the given value, so this is equivalent to allowing the brown dwarf model to evolve to various points evenly-spaced on the logarithmic x-axis of Figure 2. At the point of termination, the MESA model is saved.

Given these saved models, we next add 6 different masses to each model by setting `relax_initial_mass=.true.` and `new_mass` to values exceeding $0.07M_{\odot}$ in increments of $0.003M_{\odot}$. In addition, the new values of the mass are incremented by $-0.00015M_{\odot}$ for each value of η for visual clarity when plotting these models. The results are shown in Figures 3 and 4. Each model is shown as a series of points corresponding to different ages. For a given model, the points lie along a single vertical line corresponding either to the initial stellar mass in the case of unmodified models or the new stellar mass for the modified models. Modified models are colored different shades of red, and unmodified models use the yellow-purple col-

orbar. To plot brown dwarfs and stars with the same set of colors, the colors correspond to fractional rather than absolute ages. The last 15% of each model’s life is not shown, since the objects that reach the main sequence eventually undergo post-main-sequence evolution when they deplete their supply of hydrogen, and their trajectories in this diagram obscure the hydrogen-rich phase on which we are focusing.

The unmodified models, the same ones used to produce Figure 2, show an extremely clear transition between brown dwarfs with $M < M_{\text{HBL}}$ and stars with $M > M_{\text{HBL}}$ in both radius and effective temperature. This agrees well with standard brown dwarf evolutionary models, and has been suggested as a means of observationally determining the value of M_{HBL} (Burrows et al. 2011; Dieterich et al. 2014). The modified models show a bifurcation, with some moving to lower T_{eff} and R , and others to higher values. The warmer, larger-radii cases follow the evolution of the unmodified models in this mass-range, behaving exactly as if they had always been at this new mass. The modified models that cool and contract appear for all intents and purposes to be brown dwarfs despite having masses exceeding M_{HBL} . Their properties are a simple continuation of the sequence of brown dwarfs, despite their non-trivial evolutionary history.

3.2. Evolution

Thinking in terms of the $\psi - M$ diagram, we recall that newly-formed objects begin their life on the right

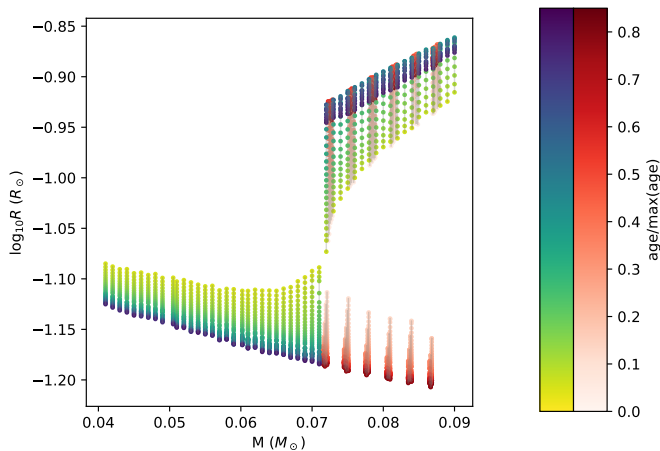


Figure 3. The mass-radius relation. The evolution of a series of MESA models evenly-spaced in initial mass (see section 2.4) is shown with a yellow-purple colorbar, where the color represents the fractional age of the model before it is eventually terminated by becoming too dense and cold to be adequately described by MESA’s equation of state. As expected, at the hydrogen burning limit, $\approx 0.07M_{\odot}$, the radius shows a sudden increase as the objects transition from brown dwarfs to main sequence stars. The red colorbar shows the evolution of a set of models where mass has been added to a brown dwarf just below the hydrogen burning limit, yielding the new masses shown in this plot. At a given mass, several different models have been run corresponding to different central degeneracies of the initial brown dwarf before mass was added to it. Some of these modified models become ordinary stars, with paths similar to the yellow-purple tracks of stars with masses above $\approx 0.07M_{\odot}$, while those with sufficiently degenerate initial conditions behave like a continuation of the sequence of ordinary brown dwarfs.

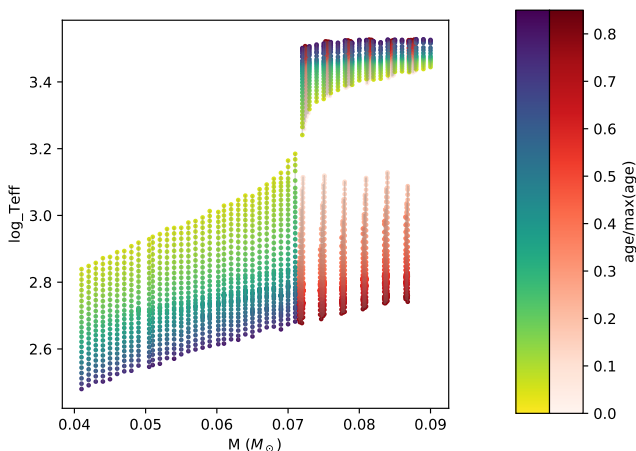


Figure 4. The mass-effective temperature relation. This diagram is constructed in the same way as Figure 3, and in fact shows essentially the same behavior. Mass added to a sufficiently degenerate brown dwarf below the hydrogen burning limit results in stars that behave like brown dwarfs above the conventional hydrogen burning limit.

hand side of this diagram. In order to make the jump across the region where $L_N > L_S$ (see Figure 1), the object would need to suddenly cool and shrink. It seems unlikely that any realistic astrophysical process would have this effect. It follows that the most plausible route to forming overmassive brown dwarfs is for an ordinary

brown dwarf, i.e. below the hydrogen burning limit, to gain mass. The key is that the brown dwarf must be sufficiently old that its value of ψ falls below ψ_{\min} , the abscissa of the hydrogen burning limit. Based on Figure 2, $\psi_{\min} \approx 0.1$, both for the analytic models and the MESA models. The isochrones suggest that the brown dwarf must be older than $\sim 3 \times 10^9$ yr for ψ to be less than ψ_{\min} .

Not only must ψ be less than ψ_{\min} when new material is added to the brown dwarf, but ψ must remain to the left of the low- ψ branch of the $L_N = L_S$ curve as the mass increases. This may be challenging because the process of adding mass to the star is likely to heat it up and increase ψ . One could imagine this process either as steady accretion or collision(s) with other objects. In the case of the former, the accretion luminosity is

$$L_a = \frac{GM}{R} \frac{dM}{dt} \quad (13)$$

If we assert that the accretion luminosity must be small compared to the luminosity along the low- ψ branch of the $L_N = L_S$ curve, we can say that the accretion rate must not exceed

$$\frac{dM}{dt} \lesssim 4.7 \times 10^{-3} \frac{M_{\odot}}{\text{Gyr}} \left(\frac{R}{0.1R_{\odot}} \right) \left(\frac{M}{0.07M_{\odot}} \right)^{-1} \left(\frac{L_a}{10^{-4}L_{\odot}} \right)^{-1} \quad (14)$$

The timescale for this accretion rate to increase the mass of the brown dwarf from $0.07M_{\odot}$ to $0.08M_{\odot}$ is 2 Gyr, implying that such objects could in principle exist in today’s universe.

This rate of accretion is, however, non-trivial to supply to a brown dwarf. The Bondi accretion rate (Bondi & Hoyle 1944) for a background number density n and relative velocity v is

$$\frac{dM}{dt} = 7.2 \times 10^{-9} \frac{M_{\odot}}{\text{Gyr}} \left(\frac{M}{0.07M_{\odot}} \right)^2 \left(\frac{n}{1 \text{ cm}^{-3}} \right) \left(\frac{v}{10 \text{ km s}^{-1}} \right)^{-3}, \quad (15)$$

so the timescale for a brown dwarf to grow at a rate approaching the limit of Equation (14) from anything resembling the Milky Way’s interstellar medium is orders of magnitude longer than the age of the universe. Interestingly the conditions in an AGN accretion disk, with $n \sim 10^9 \text{ cm}^{-3}$ and $v \sim c_s \sim 100 \text{ km s}^{-1}$ yield about the right order of magnitude for feeding the brown dwarf near the limit imposed by Equation (14). Suitable conditions may also arise in dense structures of molecular clouds, but these conditions will generally persist for far shorter than the Gyr timescales necessary to substantially grow the brown dwarf’s mass.

The most promising mechanism to substantially grow the brown dwarf’s mass on a slow enough timescale to avoid violating Condition (14), is via Roche lobe overflow in binary mass transfer. This is a well-studied theoretical problem with applications to stellar population synthesis, variable stars, and accretion onto compact objects. First, we define the mass ratio $q = M_{\text{donor}}/M_{\text{accretor}}$, where M_{accretor} is the mass of the (denser) star that is accreting mass from its companion, and M_{donor} is the mass of the star that is filling its Roche lobe and losing mass as a result. Because the size of the Roche lobe itself depends on q , transferring mass and decreasing q tends to

reduce the size of the Roche lobe. If this decrease happens too quickly, the mass loss rate can run away and proceed on a dynamical timescale. Roughly speaking, stable mass transfer requires that $q \lesssim 5/6$, with some modest dependence on how the donor star reacts to the mass loss; if the donor star can contract faster than its Roche lobe size decreases, it could transfer mass stably at somewhat larger q values.

Assuming the mass loss proceeds stably the question becomes how it is driven. A common scenario is that the donor star has begun to fill its Roche lobe as the result of post main sequence stellar evolution, and in this case the mass transfer proceeds on a nuclear timescale of the donor star. However, if $q \lesssim 5/6$, and we are attempting to add mass to a brown dwarf with initial mass $M_{\text{accretor}} \approx M_{\text{HBL}} \approx 0.07M_{\odot}$, there is no nuclear timescale, and in fact the donor object is cooling and contracting. Something else must therefore be invoked to get the donor star to fill its Roche lobe.

An obvious candidate is for the binary to lose angular momentum due to the radiation of gravitational waves. This possibility was first pointed out by Kraft et al. (1962), and employed in simple models by Paczyński (1967) and Faulkner (1971). In these models, the time derivative of the angular momentum J is set equal to the rate at which angular momentum is lost by gravitational waves \dot{J}_{GW} , where

$$J = GM_{\text{donor}}M_{\text{accretor}}\sqrt{Ga/M_{\text{tot}}}, \quad (16)$$

$M_{\text{tot}} = M_{\text{donor}} + M_{\text{accretor}}$, a is the orbital separation between the two objects, and, from Peters (1964) or Landau & Lifshitz (1975),

$$\dot{J}_{\text{GW}} = -\frac{32}{5c^5}M_{\text{donor}}^2M_{\text{accretor}}^2\sqrt{\frac{G^7M_{\text{tot}}}{a^7}}. \quad (17)$$

As presently-formulated, this problem appears to be a single evolution equation, $dJ/dt = \dot{J}_{\text{GW}}$, with three independent unknown variables: M_{donor} , M_{accretor} , and a . We can of course employ the reasonable assumption that mass is conserved in the system to re-express all the masses as appropriate combinations of q and the constant M_{tot} , i.e. $M_{\text{donor}} = M_{\text{tot}}q(1+q)^{-1}$ and $M_{\text{accretor}} = M_{\text{tot}}(1+q)^{-1}$.

Finally, to eliminate a from the evolution equation, we follow Faulkner (1971) and make the assumption that there is a powerlaw mass-radius relation that applies for the donor star, namely $R_{\text{donor}} = \mathcal{R}M_{\text{donor}}^n$, and that throughout the evolution $R_{\text{donor}} = R_{L,\text{donor}}$, the radius of a sphere whose volume is the same as the Roche volume. Eggleton (1983) derived a convenient numerical expression for this quantity as a function of a and q , namely

$$\frac{R_{L,\text{donor}}}{a} = \frac{0.49q^{2/3}}{0.6q^{2/3} + \log(1+q^{1/3})}. \quad (18)$$

Following this chain of relations, all values of a may be replaced with functions of M_{donor} , which may in turn be replaced with functions of q , leaving an evolution equation for q alone, depending on the total mass of the system, and the normalization and slope of the mass-radius

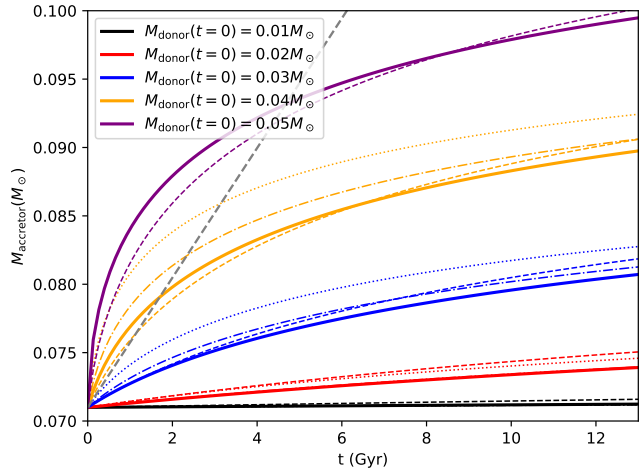


Figure 5. Growth of a brown dwarf via gravitational wave regulated Roche lobe overflow. The mass of the accreting brown dwarf is shown as a function of time for different initial companion masses (different colors), and for slightly different assumptions about the mass-radius relation (different linestyles). These are $R_0 = 10^{-1.08}R_{\odot}$, $n = -0.1$ (solid), $R_0 = 10^{-1.03}R_{\odot}$, $n = 0.1$ (dashed), $R_0 = 10^{-1.13}R_{\odot}$, $n = -0.2$ (dash-dotted), and $R_0 = 10^{-1.2}R_{\odot}$, $n = -0.28$ (dotted), covering the range of values for these parameters as the brown dwarfs modeled with MESA age. In addition, a straight grey dashed line shows roughly the maximum growth rate of the accreting brown dwarf such that its interior remains sufficiently degenerate to keep the object an overmassive brown dwarf rather than a new star.

relationship.

$$\frac{dq}{dT} = \frac{-1}{F'(q)}(1+q)^{7n/2-4}q^{2-7n/2}\mathcal{G}(q)^{7/2}, \quad (19)$$

where $\mathcal{G}(q)$ is simply the right-hand side of Equation (18), and $F'(q) = dF/dq$ is the derivative of

$$F = (1+q)^{-2-n/2}q^{1+n/2}\mathcal{G}(q)^{-1/2}. \quad (20)$$

Equation (19) has also been non-dimensionalized by rescaling the time variable as

$$t = T\mathcal{R}^4\frac{5c^5}{32}G^{-3}M_{\text{tot}}^{4n-3}. \quad (21)$$

Equation (19) can be evolved numerically for any initial q and any value of n , then redimensionalized to obtain, e.g. $M_{\text{accretor}}(t)$. We do this for a variety of donor mass values, and reasonable values for n and \mathcal{R} . For convenience we define $R_0 = \mathcal{R}/(0.071M_{\odot})^n$, the value of the donor star's radius if the mass-radius relation were extrapolated to a mass of $0.071M_{\odot}$. The result is shown in Figure 5.

Over the range of values we have chosen for the mass-radius relationship, the growth of mass for the accreting brown dwarf is relatively insensitive to these parameters. The primary driver controlling how quickly mass is transferred is the total mass of the system. For an initial brown dwarf mass of $0.07M_{\odot}$, the maximum mass the companion brown dwarf may have to maintain stable mass transfer is not much larger than $0.05M_{\odot}$. In this case, the mass of the accreting brown dwarf could conceivably grow by about 50%, up to about $0.1M_{\odot}$. However, in addition to various scenarios for the growth

of the accreting brown dwarf, Figure 5 shows a straight diagonal line representing the mass growth of a brown dwarf marginally obeying condition (14), namely that the accretion rate should be low enough that the accretion luminosity does not exceed the intrinsic luminosity of the object. For the largest values of M_{donor} , this line is crossed, indicating that the accretion rates early in the evolution of these systems are high enough to potentially heat up the accreting brown dwarf and push it into the regime of ordinary stellar evolution for an object of that mass. However, once the initial donor mass falls below about $0.04M_{\odot}$, the mass transfer proceeds sufficiently slowly at all times that the brown dwarf may grow in mass by $\sim 10\%$, exceeding M_{HBL} while remaining a brown dwarf in every other respect.

The problem of binary mass transfer is certainly more complicated than this simple model captures. There may be additional physics involved, including tides, spin, and magnetic fields, in addition to differences in the physics of brown dwarfs imposed by having the donor star fill its Roche lobe and having both stars rotating. (e.g. Hurley et al. 2002; Paxton et al. 2015) We defer a fuller treatment of this problem to later work; for now it suffices to show that there is a plausible means by which overmassive brown dwarfs may exist in the present-day universe.

Other possibilities for adding mass to brown dwarfs include capture of stellar wind material from a massive companion, the complete or partial tidal disruption of neighboring objects, and collisions. Although each of these scenarios entails substantial uncertainty, we estimate that each one is fairly unlikely to produce the bulk of the putative overmassive brown dwarf population. Capture of stellar wind material occurs when the brown dwarf is in a binary system with a more massive star that is losing mass in a stellar wind. If mass is accreted following the prescription of Bondi & Hoyle (1944), given a mass loss rate from the donor star from Nieuwenhuijzen & de Jager (1990), and assuming that the wind velocity is of order the escape velocity from the surface of the donor star, we find that the maximum mass accreted by the brown dwarf over the course of the life of the donor star never exceeds a few times $10^{-5}M_{\odot}$. This maximum occurs when the separation is as close as possible without running into the Roche limit, and the mass of the donor is large enough for the mass transfer rate to approach the limit of Condition (14). At higher masses, the accretion rate is too great to keep the brown dwarf cool, and at closer separations the donor star loses mass directly via tidal perturbation. This intersection occurs at about $M_{\text{donor}} \approx 13M_{\odot}$ and $a \approx 10^{11}$ cm. Fundamentally this mechanism will have a difficult time transferring enough mass to the brown dwarf to make a difference because in order for the mass transfer rate to be large enough to be relevant, the donor star must be so massive that its lifetime is far shorter than the 2 Gyr necessary to transfer $\sim 10^{-2}M_{\odot}$.

It is also worth considering tidal disruption events, wherein some object passes sufficiently close to the brown dwarf that tidal forces rip the donor object apart. Tidal disruptions are well-studied in the case of stars interacting with supermassive black holes at the centers of galaxies (e.g. Rees 1988; Guillochon & Ramirez-Ruiz 2013). Since brown dwarfs just below the hydrogen burning limit lie at a minimum in the mass-radius relation (see

e.g. Figure 3) they may in principle tidally disrupt other objects. In the MESA models just below the hydrogen burning limit, the mean density of the brown dwarf reaches about 200 g cm^{-3} . This implies a tidal radius of about

$$r_t \approx 3 \times 10^{10} \text{ cm} \left(\frac{\rho_{\text{sat}}}{1 \text{ g cm}^{-3}} \right)^{-1/3} \quad (22)$$

for satellites of mean density ρ_{sat} .

Tidal disruptions occur on a dynamical timescale, with the accretion potentially spread out by the viscous and collisional dynamics of the bound tidal stream. Nonetheless, the timescale for this process is quite short. In order to feed the brown dwarf sufficiently slowly, one could instead imagine a process analogous to that presented in MacLeod et al. (2013). In that scenario, an evolved star on an eccentric orbit is partially tidally disrupted during each pericenter passage, and as a result its radius expands preparing it for another partial tidal disruption on its next orbit. The evolutionary timescale of an evolved star is too short for our purposes, but we could imagine instead that the companion star is on the main sequence with a mass of order $1M_{\odot}$. Such a star has too large a radius to fit within r_t , but the tidal forces may be sufficient to transfer part of the outer layers of the star without such a close pericenter passage (MacLeod et al. 2013). While it may be uncommon for a brown dwarf to find itself with a larger stellar companion on an eccentric orbit just right for this partial tidal disruption to occur, this scenario may be worth further consideration.

4. DISCUSSION

We have established that brown dwarfs with masses exceeding the hydrogen burning limit may in principle exist in the universe today, and the most promising means to create them is Roche lobe overflow in compact binary brown dwarf systems. We now turn to the question of the implications, both in interpreting observational data, and empirically constraining the frequency of overmassive brown dwarfs.

Binary brown dwarf systems are highly prized for their power in calibrating the evolutionary models mentioned in the introduction. Since it is possible to measure the mass of one or both components of a binary dynamically, relationships between stellar mass and spectral type can be determined directly, and degeneracies in model predictions of stellar properties may be broken (see Dupuy & Liu 2017). Binary brown dwarfs are doubly important in the context of overmassive brown dwarfs, since binaries are likely necessary for their formation, and definitively confirming their existence independent of spectral models will likely require a dynamical mass measurement.

The fraction of brown dwarfs in visually-resolved binaries with separations exceeding about 3 AU is approximately 10% (Burgasser 2007). The true binary fraction may be somewhat higher, but based on a small sample of brown dwarfs monitored with radial velocity, Joergens (2008) estimate that the true binary fraction is unlikely to exceed 20%, consistent with the trend that lower-mass stars have lower binary fractions (e.g. Duquennoy & Mayor 1991; Yuan et al. 2015). There is also some evidence (Allers 2012) that brown dwarf binaries preferentially have mass ratios close to unity, which poses

an additional barrier to our stable binary mass transfer scenario. This suggests that the ultracompact binaries necessary to produce overmassive brown dwarfs are rare, with the bulk of brown dwarf binaries being too wide to transfer mass in the course of their lifetimes, too close to equal mass ratios, and brown dwarf binaries as a whole being reasonably uncommon.

We can make a very rough estimate of the frequency of Roche lobe overflow events among the brown dwarf population as follows. Differentiating the definition of the total angular momentum of the binary system, we see that in the absence of mass transfer $\dot{a}/a = 2\dot{J}/J$. If we assume gravitational waves are the dominant sink of orbital angular momentum and plug in the definitions of J and \dot{J}_{GW} , we can find how far the binary shrinks over some time t analytically. In particular, if the binary ends up at a final separation a_f , it must have started at a separation of

$$a_0 = \left(a_f^4 + \frac{256G^3}{5c^5} M_1 M_2 (M_1 + M_2) t \right)^{1/4} \quad (23)$$

Setting the final separation to be equal to the radius at which the donor star begins to overflow its Roche lobe, namely $a_f = R_{\text{donor}}/\mathcal{G}(q)$ in the parlance of the previous section, and fixing t to be the typical age of stars in the solar neighborhood, i.e. about 5 Gyr, we can determine the separation a_0 out to which some initial population of binaries would be interacting via Roche lobe overflow today. Next, we can assume some simple distribution for the initial separation of the binaries. This will depend on their formation mechanism and is poorly constrained by existing data, so for simplicity we adopt a log-uniform distribution, not dissimilar to the separation distribution of M dwarfs (Fischer & Marcy 1992) extending from a_f all the way through the empirical maximum separation of $a_{\text{max}} \sim 30$ AU. The fraction of brown dwarfs interacting via Roche lobe overflow f_{RLOF} would then be

$$f_{\text{RLOF}} = f_{\text{bin}} \frac{\ln(a_0/a_f)}{\ln(a_{\text{max}}/a_f)}. \quad (24)$$

For binaries where the accretor is $0.06\text{--}0.07 M_{\odot}$ and the donor is about $0.05 M_{\odot}$, we find $f_{\text{RLOF}} \sim 10^{-2}$ assuming $f_{\text{bin}} = 20\%$.

There are only about 10^4 brown dwarfs known in all (Burgasser et al. 2015), and these are largely discovered via wide-field surveys, e.g. WISE (Wright et al. 2010). It is possible that $\sim 10^2$ overmassive brown dwarfs are hidden among this sample if $f_{\text{RLOF}} \sim 10^{-2}$, depending on the intrinsic distribution of separations. Regardless of f_{RLOF} , it is currently quite difficult to determine whether a particular brown dwarf is in this phase. Binaries which are too compact to separate by their visual separation may still be identified in a few ways: the Doppler effect, eclipses, photometric variability, and through large discrepancies between expectations for single stars and observational data.

The Doppler effect requires expensive spectroscopic monitoring of these faint stars, and so has been restricted to reasonably small samples. However, binaries interacting via Roche lobe overflow have sufficiently short periods and large velocities that these systems should be relatively easy to find, with no need for long-term monitoring

or extremely high spectroscopic precision. LSST⁴ is expected to discover ~ 7 eclipsing binary brown dwarfs (see chapter 6.9 of LSST Science Collaboration et al. 2009). These systems will have immense constraining power on evolutionary models, and with luck ~ 1 of these systems may be a RLOF system. Sufficiently precise photometry may also reveal tight binaries (Faigler & Mazeh 2011; Millholland & Laughlin 2017), though it is unclear what the yield from LSST will be.

Another possibility for uncovering binaries is identifying outliers in observational relations appropriate for single brown dwarfs. A number of examples are discussed in some detail in Dupuy & Liu (2017), including 2MASS J0920+3517B (Kirkpatrick et al. 2000; Burgasser et al. 2006) an object which routinely appears as an outlier in the scaling relations presented in that work, and interpreted as an unresolved binary system. We caution though that overmassive brown dwarfs may also appear in observational relations outside the region expected for conventional brown dwarfs.

Another interesting consequence of our current observational understanding of brown dwarf binaries is that binaries that undergo unstable mass transfer are likely to be more common than those undergoing the stable mass transfer with $q \lesssim 5/6$ necessary to produce overmassive brown dwarfs. Binaries that undergo unstable mass transfer should very quickly, on a dynamical timescale, genuinely produce a new star provided the combined mass of the system exceeds the hydrogen burning limit. This sort of process has been considered as the dominant source of star formation in the distant future (Adams & Laughlin 1997) long after even the lowest-mass stars have died (Laughlin et al. 1997). However, nothing prevents events like this from occurring in the present-day universe as well. While the event itself may be short, the newly-extant star where only a faint brown dwarf had existed just prior may be detectable in forthcoming transient surveys such as LSST. The frequency of such events may provide an efficient complementary alternative to spectroscopic monitoring as a means to constrain the population of brown dwarf binaries. Dynamical mass transfer may also leave remnants of the donor object in analogy to “black widow” pulsars (Bailes et al. 2011) which may be detected in searches for planets around M dwarfs such as MEarth (Nutzman & Charbonneau 2008; Berta et al. 2012).

5. SUMMARY

According to conventional wisdom the dividing line between stars and brown dwarfs is very clear: there is a mass, the hydrogen burning limit, below which hydrostatic objects cannot support long-term hydrogen burning in their cores. Instead they are supported by degeneracy pressure as they cool and contract. These are brown dwarfs. Above this critical mass, objects may reach a steady state where they are supported against collapse, at least in part, by thermal pressure powered by steady hydrogen burning in their core. In this work we have shown that there are in principle objects in the universe that behave for all intents and purposes like brown dwarfs, but have masses exceeding the hydrogen burning limit.

⁴ <https://www.lsst.org/>

Brown dwarfs in this category, which we call overmassive brown dwarfs, may exist so long as their central degeneracy is large. When this is the case, the object's surface luminosity exceeds the nuclear luminosity it can generate, and the object steadily cools becoming more degenerate in the process. If the object's degeneracy is insufficiently large, its nuclear luminosity will exceed its surface luminosity, forcing the object to quickly increase its surface luminosity, and bringing it back to the main sequence of hydrogen burning and a track of ordinary stellar evolution.

Practically speaking, in order to produce a overmassive brown dwarf, an old ($\gtrsim 3$ Gyr) ordinary brown dwarf that has cooled far enough for its degeneracy to exceed some critical value must gain mass. The rate of mass gain must be large enough to substantially alter the brown dwarf's mass, but not so large that the liberation of gravitational energy associated with the accretion heats up the star's interior and decreases its central degeneracy below the critical value. We estimate that this requires an accretion rate below about $4.7 \times 10^{-3} M_{\odot} \text{ Gyr}^{-1}$, which means it takes at least 2 Gyr to increase the object's mass by $0.01 M_{\odot}$, a substantial amount for a $\approx 0.07 M_{\odot}$ object. In the lifetime of the universe, an overmassive brown dwarf could in principle reach about $0.12 M_{\odot}$ if it can grow continuously at the maximum rate for 10 Gyr following the ~ 3 Gyr of cooling necessary to become sufficiently degenerate.

A number of physical processes may allow mass transfer on about the right timescale. We consider the most promising to be Roche lobe overflow in a compact brown dwarf-brown dwarf binary driven by the radiation of gravitational waves. This scenario, and the other plausible alternatives that we have considered, is likely to be rare, but exactly how rare depends on poorly-constrained properties of brown dwarf binaries. LSST will likely yield a handful of eclipsing binary brown dwarfs which could include an example of a pair interacting via Roche lobe overflow. Photometric variability from non-eclipsing binaries, and short-term low-precision radial velocity surveys are also potential routes to discover systems undergoing Roche lobe overflow and overmassive brown dwarfs.

ACKNOWLEDGEMENTS

This work was supported in part by an ITC Fellowship (JCF) and grants from the Breakthrough Prize Foundation and the John Templeton Foundation (AL). This work has benefited from helpful conversations with Morgan MacLeod, Jieun Choi, Sayantan Auddy, and Adam Burrows. In addition to MESA, we have used a variety of free resources including matplotlib (Hunter 2007), numpy and scipy (Oliphant 2007), NASA ADS and the arXiv.

REFERENCES

- Ackerman A. S., Marley M. S., 2001, *The Astrophysical Journal*, 556, 872
- Adams F. C., Laughlin G., 1997, *Reviews of Modern Physics*, 69, 337
- Allard F., Hauschildt P. H., Alexander D. R., Starrfield S., 1997, *Annual Review of Astronomy and Astrophysics*, 35, 137
- Allers K. N., 2012, pp 105–110
- Auddy S., Basu S., Valluri S. R., 2016, *Advances in Astronomy*, 2016, 574327
- Bailes M. et al., 2011, *Science*, 333, 1717
- Baraffe I., Chabrier G., Allard F., Hauschildt P. H., 1995, *The Astrophysical Journal Letters*, 446, L35
- Baraffe I., Chabrier G., Barman T. S., Allard F., Hauschildt P. H., 2003, *Astronomy and Astrophysics*, 402, 701
- Baraffe I., Homeier D., Allard F., Chabrier G., 2015, *Astronomy and Astrophysics*, 577, A42
- Berta Z. K., Irwin J., Charbonneau D., Burke C. J., Falco E. E., 2012, *The Astronomical Journal*, 144, 145
- Bondi H., Hoyle F., 1944, *Monthly Notices of the Royal Astronomical Society*, 104, 273
- Burgasser A. J., 2007, *The Astrophysical Journal*, 659, 655
- Burgasser A. J., Geballe T. R., Leggett S. K., Kirkpatrick J. D., Golimowski D. A., 2006, *The Astrophysical Journal*, 637, 1067
- Burgasser A. J. et al., 2015, *The Astrophysical Journal Supplement Series*, 220, 18
- Burrows A., Heng K., Nampaisarn T., 2011, *The Astrophysical Journal*, 736, 47
- Burrows A., Hubbard W. B., Lunine J. I., Liebert J., 2001, *Reviews of Modern Physics*, 73, 719
- Burrows A., Hubbard W. B., Saumon D., Lunine J. I., 1993, *The Astrophysical Journal*, 406, 158
- Burrows A., Liebert J., 1993, *Reviews of Modern Physics*, 65, 301
- Burrows A. et al., 1997, *The Astrophysical Journal*, 491, 856
- Chabrier G., 2003, *Publications of the Astronomical Society of the Pacific*, 115, 763
- Chabrier G., Baraffe I., 1997, *Astronomy and Astrophysics*, 327, 1039
- Chabrier G., Baraffe I., Allard F., Hauschildt P., 2000, *The Astrophysical Journal*, 542, 464
- Chabrier G., Saumon D., Hubbard W. B., Lunine J. I., 1992, *The Astrophysical Journal*, 391, 817
- Choi J., Dotter A., Conroy C., Cantiello M., Paxton B., Johnson B. D., 2016, *The Astrophysical Journal*, 823, 102
- Cooke R. J., Pettini M., Nollett K. M., Jorgenson R., 2016, *The Astrophysical Journal*, 830, 148
- Cushing M. C. et al., 2008, *The Astrophysical Journal*, 678, 1372
- Dieterich S. B., Henry T. J., Jao W.-C., Winters J. G., Hosey A. D., Riedel A. R., Subasavage J. P., 2014, *The Astronomical Journal*, 147, 94
- Dupuy T. J., Liu M. C., 2017, *The Astrophysical Journal Supplement Series*, 231, 15
- Duquennoy A., Mayor M., 1991, *Astronomy and Astrophysics*, 248, 485
- Eggleton P. P., 1983, *The Astrophysical Journal*, 268, 368
- Faigler S., Mazeh T., 2011, *Monthly Notices of the Royal Astronomical Society*, 415, 3921
- Faulkner J., 1971, *The Astrophysical Journal Letters*, 170, L99
- Ferguson J. W., Alexander D. R., Allard F., Barman T., Bodnarik J. G., Hauschildt P. H., Heffner-Wong A., Tamanai A., 2005, *The Astrophysical Journal*, 623, 585
- Fischer D. A., Marcy G. W., 1992, *The Astrophysical Journal*, 396, 178
- Fowler W. A., Caughlan G. R., Zimmerman B. A., 1975, *Annual Review of Astronomy and Astrophysics*, 13, 69
- Graboske H. C., Dewitt H. E., Grossman A. S., Cooper M. S., 1973, *The Astrophysical Journal*, 181, 457
- Guillochon J., Ramirez-Ruiz E., 2013, *The Astrophysical Journal*, 767, 25
- Hayashi C., Nakano T., 1963, *Progress of Theoretical Physics*, 30, 460
- Hunter J. D., 2007, *Computing in Science Engineering*, 9, 90
- Hurley J. R., Tout C. A., Pols O. R., 2002, *Monthly Notices of the Royal Astronomical Society*, 329, 897
- Joergens V., 2008, *Astronomy and Astrophysics*, 492, 545
- Kirkpatrick J. D. et al., 2000, *The Astronomical Journal*, 120, 447
- Kraft R. P., Mathews J., Greenstein J. L., 1962, *The Astrophysical Journal*, 136, 312
- Kumar S. S., 1963, *The Astrophysical Journal*, 137, 1121
- Landau L. D., Lifshitz E. M., 1975, *The Classical Theory of Fields*
- Laughlin G., Bodenheimer P., 1993, *The Astrophysical Journal*, 403, 303
- Laughlin G., Bodenheimer P., Adams F. C., 1997, *The Astrophysical Journal*, 482, 420
- LSST Science Collaboration et al., 2009, *ArXiv e-prints*, 0912, arXiv:0912.0201
- MacDonald J., Mullan D. J., 2009, *The Astrophysical Journal*, 700, 387

- MacLeod M., Ramirez-Ruiz E., Grady S., Guillochon J., 2013, *The Astrophysical Journal*, 777, 133
- Marley M. S., Robinson T. D., 2015, *Annual Review of Astronomy and Astrophysics*, 53, 279
- Millholland S., Laughlin G., 2017, *The Astronomical Journal*, 154, 83
- Morley C. V., Fortney J. J., Marley M. S., Visscher C., Saumon D., Leggett S. K., 2012, *The Astrophysical Journal*, 756, 172
- Nieuwenhuijzen H., de Jager C., 1990, *Astronomy and Astrophysics*, 231, 134
- Nutzman P., Charbonneau D., 2008, *Publications of the Astronomical Society of the Pacific*, 120, 317
- Oliphant T. E., 2007, *Computing in Science and Engg.*, 9, 10
- Paczynski B., 1967, *Acta Astronomica*, 17, 287
- Paxton B., Bildsten L., Dotter A., Herwig F., Lesaffre P., Timmes F., 2011, *The Astrophysical Journal Supplement Series*, 192, 3
- Paxton B. et al., 2013, *The Astrophysical Journal Supplement Series*, 208, 4
- Paxton B. et al., 2015, *The Astrophysical Journal Supplement Series*, 220, 15
- Peters P. C., 1964, *Physical Review*, 136, B1224
- Rebolo R., Zapatero Osorio M. R., Martín E. L., 1995, *Nature*, 377, 129
- Rees M. J., 1988, *Nature*, 333, 523
- Saumon D., Bergeron P., Lunine J. I., Hubbard W. B., Burrows A., 1994, *The Astrophysical Journal*, 424, 333
- Saumon D., Marley M. S., 2008, *The Astrophysical Journal*, 689, 1327
- Tsuji T., Ohnaka K., Aoki W., Nakajima T., 1996, *Astronomy and Astrophysics*, 308, L29
- Wright E. L. et al., 2010, *The Astronomical Journal*, 140, 1868
- Yuan H., Liu X., Xiang M., Huang Y., Chen B., Wu Y., Hou Y., Zhang Y., 2015, *The Astrophysical Journal*, 799, 135